Supplementary Information

Unveiling the crystal and magnetic texture of iron oxide nanoflowers

Carlos Moya,[a,b]* Mariona Escoda-Torroella,[a,b] Javier Rodríguez-Álvarez,[a,b] Adriana I. Figueroa,[a,b] Íker García,[a] Inés Batalla Ferrer-Vidal,[a] A. Gallo-Cordova,[c] M. Puerto Morales,[c] Lucía Aballe,[d] Arantxa Fraile Rodríguez,[a,b] Amílcar Labarta, [a,b] and Xavier Batlle [a,b]

[a] Departament de Física de la Matèria Condensada, Universitat de Barcelona, Martí i Franquès 1, 08028 Barcelona, Spain

[b] Institut de Nanociència i Nanotecnologia (IN2UB), Universitat de Barcelona, 08028 Barcelona, Spain

[c] Department of Nanoscience and Nanotechnology, Instituto de Ciencia de Materiales de Madrid (ICMM-CSIC), Sor Juana Inés de la Cruz 3, 28049 Madrid, Spain

[d] ALBA Synchrotron Light Facility, CELLS, 08290 Barcelona, Spain

Corresponding authors: carlosmoyaalvarez@ub.edu, xavierbatlle@ub.edu

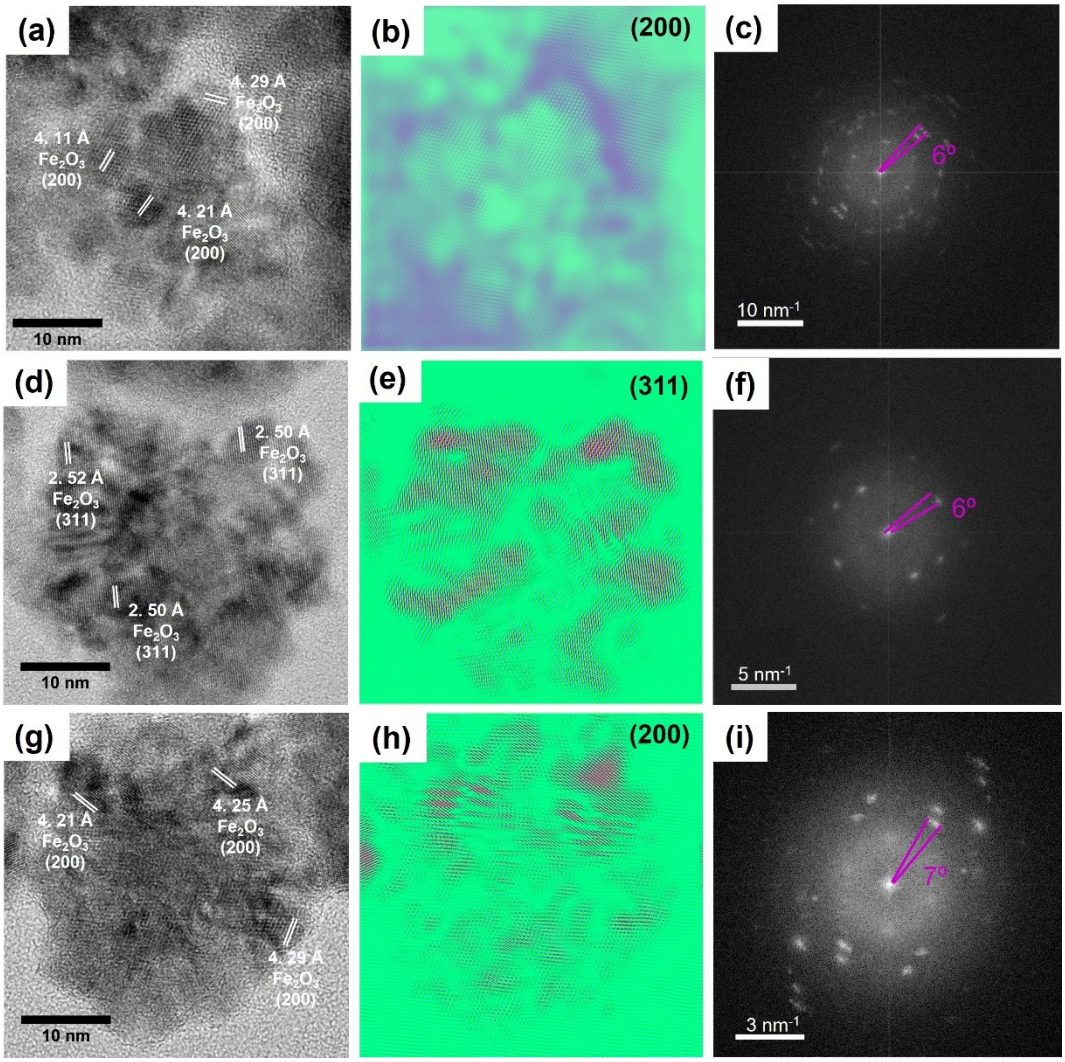

Figure S1. HRTEM Gallery of IONF40. The first column shows HRTEM images of single IONF showing γ-Fe_2O_3 crystal planes. The second column shows reconstructed images obtained by inverting the FFT of filtered FFT images, containing only features associated with the (200) and (311) planes. The third column shows average angles subtended by the arcs of the spots in the FFT patterns.

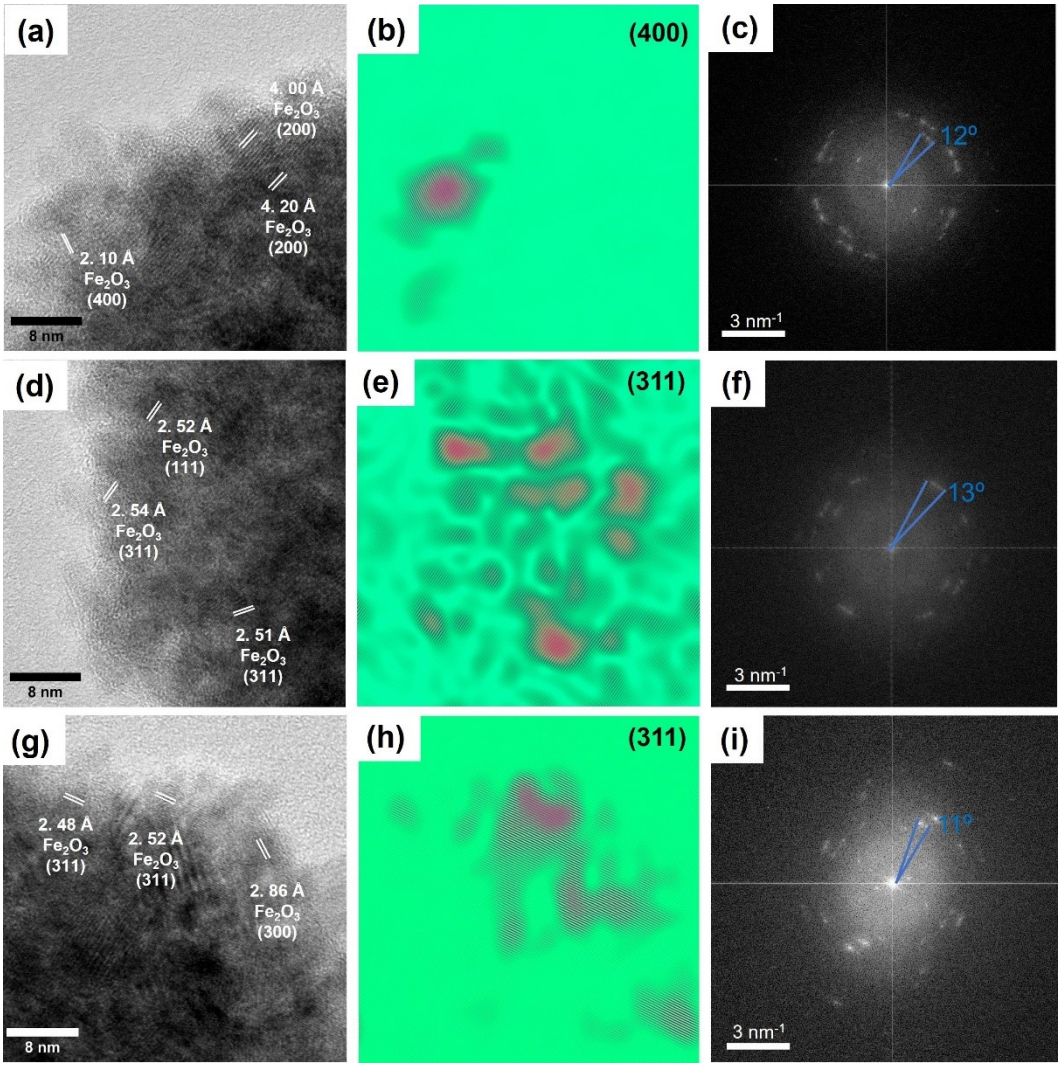

Figure S2. HRTEM images of IONF100. The first column shows small areas of single IONF revealing their γ-Fe_2O_3 crystal planes. Reconstructed images of the (311) and (400) crystal planes, obtained by inverting the FFT of filtered FFT images, are shown in the second column. The third column shows the average angles subtended by the arcs of the spots in the FFT patterns.

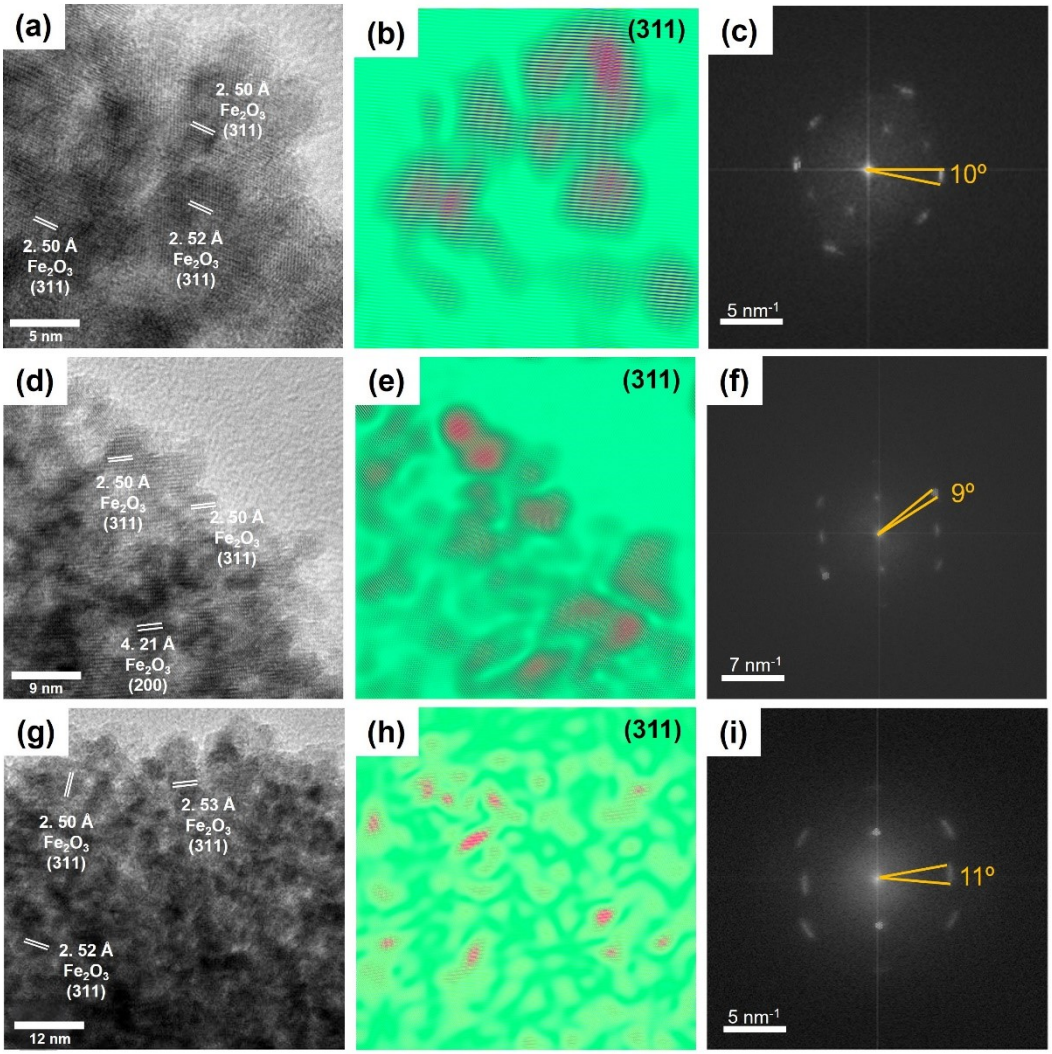

Figure S3. HRTEM Gallery of IONF400. First column shows HRTEM images of single IONF400, revealing their γ-Fe_2O_3 crystal planes. Reconstructs images of the (311) planes, obtained by inverting the FFT of filtered FFT images, are shown in the second column. The third column shows the average angles subtended by the arcs of the spots in the FFT patterns.

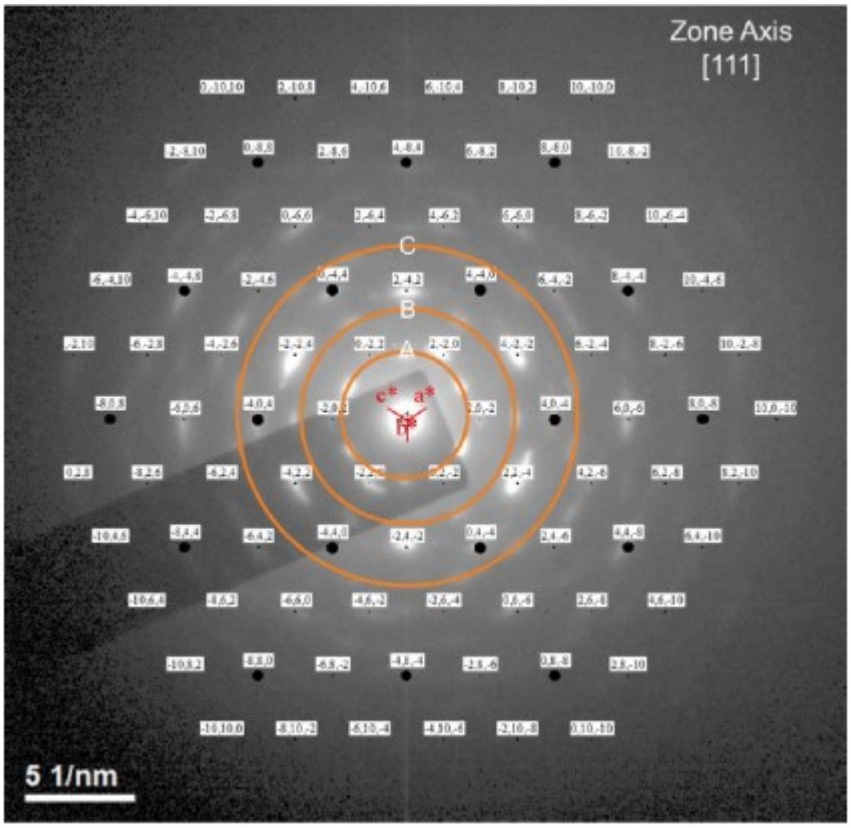

Figure S4. Analysis of the SAED pattern for sample IONF400 including the indexation of the spots corresponding to the [111] zone axis. Orange circles highlight those spots not belonging to the [111] zone axis which are indexed in Table S1.

Table S1. Study of the interplanar distances (dhkl) for sample IONF400 from the SAED analysis.

Sample	Ring	Experimental d_{hkl} (Å)	Plane of γ-Fe_2O_3
IONF400	A	3.48	2 1 1
		2.99	2 2 0
	B	2.01	4 0 0
		1.75	4 2 2
		1.51	4 4 0
	C	1.31	6 2 0
		1.14	6 4 2
		1.01	6 6 0
		0.89	8 4 4
		0.84	8 6 2
		0.66	8 2 10

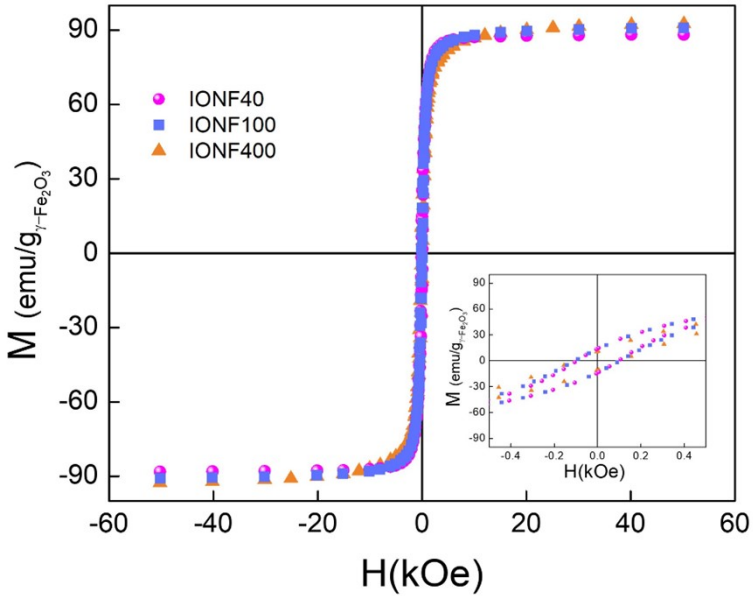

Figure S5. Hysteresis loops at 5 K of samples in powder recorded within H= ±50 kOe. The inset shows the detail corresponding to a small range of the magnetic field around the origin. Symbols are as follows: IONF40 (magenta solid spheres), IONF100 (blue solid squares), and IONF400 (orange solid triangles).

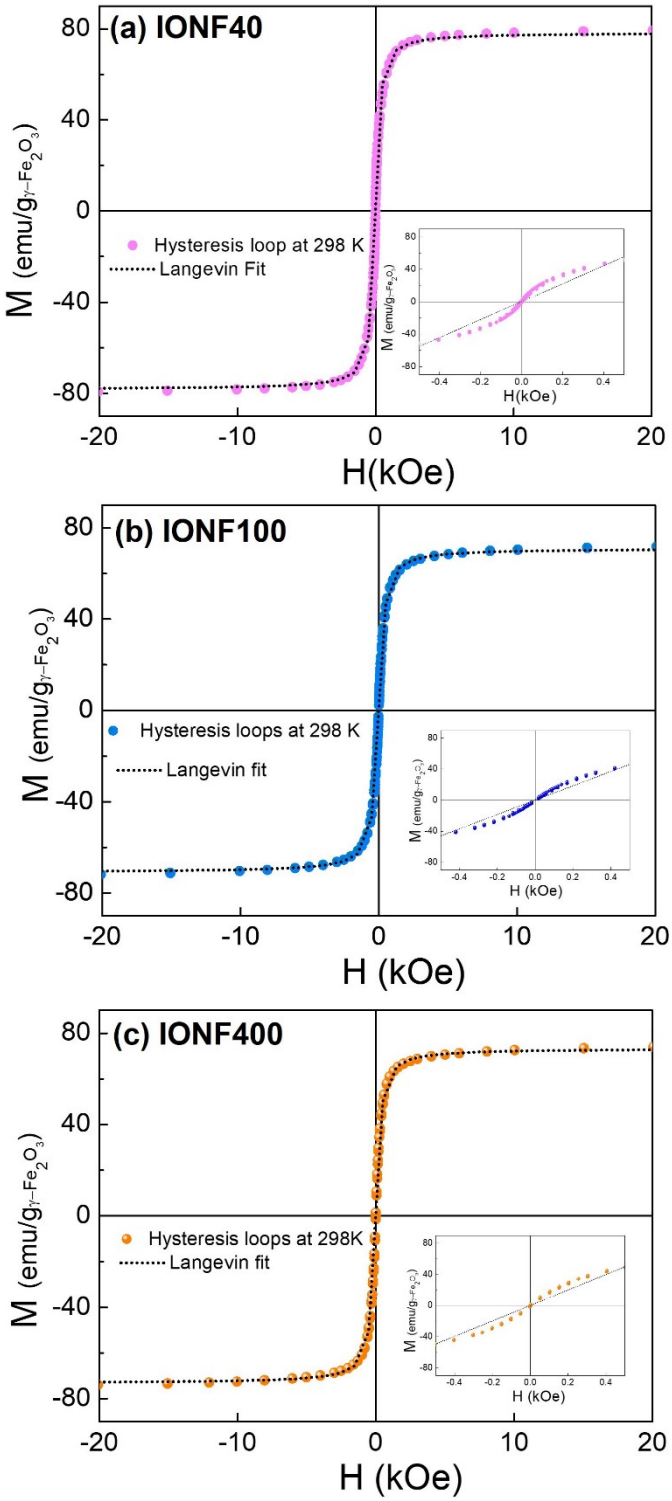

Figure S6. Langevin fitting of the experimental magnetization at 298 K for samples IONF40 (a), IONF100 (b), and IONF400 (c). The averaged experimental data for samples IONF40, IONF100, and IONF400 are plotted as magenta, blue, and orange spheres, respectively. The black dotted lines correspond to the fitted curves. Insets show the low field region of M-H loops around the origin.

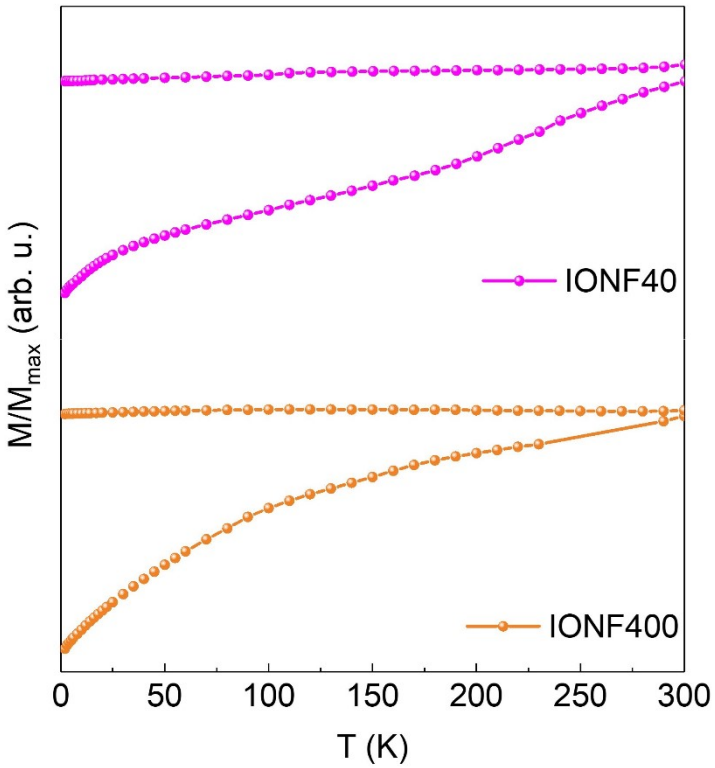

Figure S7. M_{ZFC}/M_{FC} curves measured under 50 Oe for samples IONF40 (magenta spheres) and IONF400 (orange spheres).

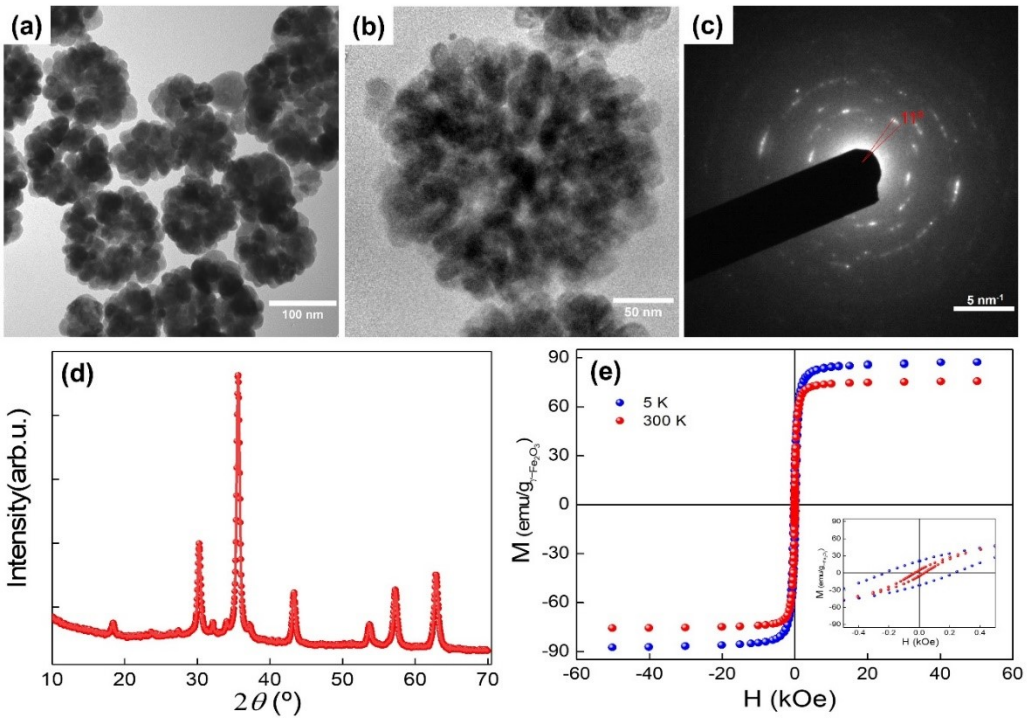

Figure S8. Graphical summary of the structural and magnetic characterization of sample IONF200. (a) Low-magnification TEM image showing some few of IONF200 arranged on the TEM grid. (b) HRTEM image of a single IONF200 and (c) its corresponding SAED pattern showing an average angle subtended by the arcs of the spots of 11º. (d) XRD spectrum and fitted curve showed with red spheres and a red solid line, respectively. (e) Hysteresis loops at 5 and 298 K depicted with blue and red spheres, respectively. Inset shows the detail of the curves within the low magnetic field region around the origin.

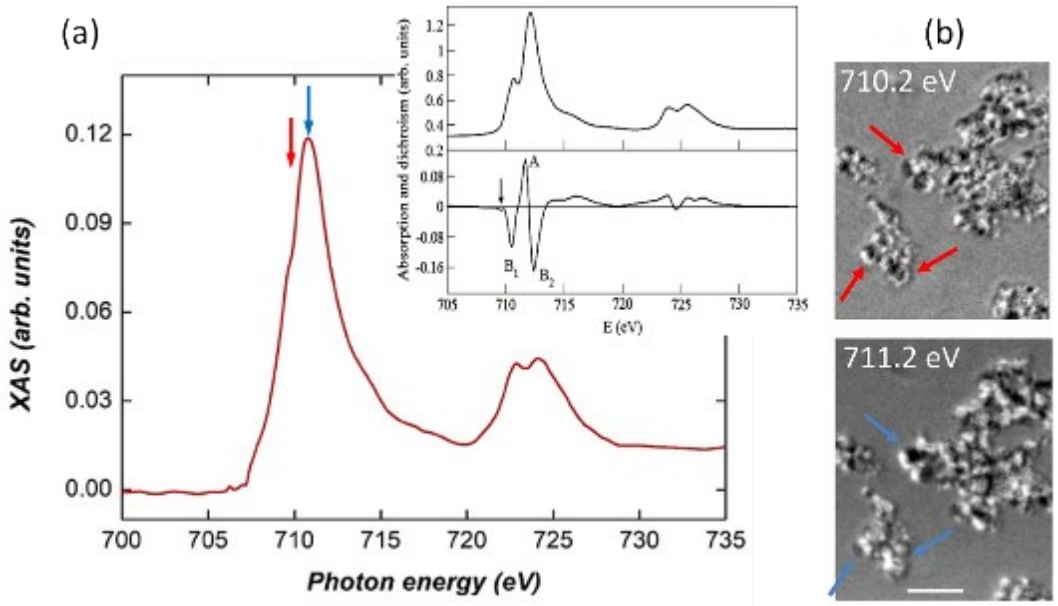

Figure S9. (a) Local isotropic XAS from a single IONF, as obtained by collecting stacks of 2D images around the Fe $L_{3,2}$ edges for both circular polarizations. A flat field image was recorded at each energy point to normalize the data. Local XAS determines the energy that gives the largest magnetic contrast for subsequent 2D tomographic imaging and confirms the exact phase composition across the whole IONF volume. Comparison with the typical aspect of XAS and XMCD recorded on reference γ-Fe_2O_3 NP reported in the literature and shown in the inset (figure adapted from [28]), seems to confirm the presence of the maghemite phase (γ-Fe_2O_3) in the IONF, as determined from both XRD spectra (see main text) and the absence of any anomaly associated with the Verwey transition in the ZFC-FC data. Red and blue lines mark the position of peaks A and B_2, that take place at 710.2 and 711.2 eV, respectively. (b) Magnetic TXM images recorded at 710 eV (top) and 711.2 eV (bottom) corresponding to peaks A and B_2, respectively, in the inset in (a). The occurrence of magnetic contrast reversal is clear, as depicted in the regions pointed by arrows. Scale bar is 2 μm.

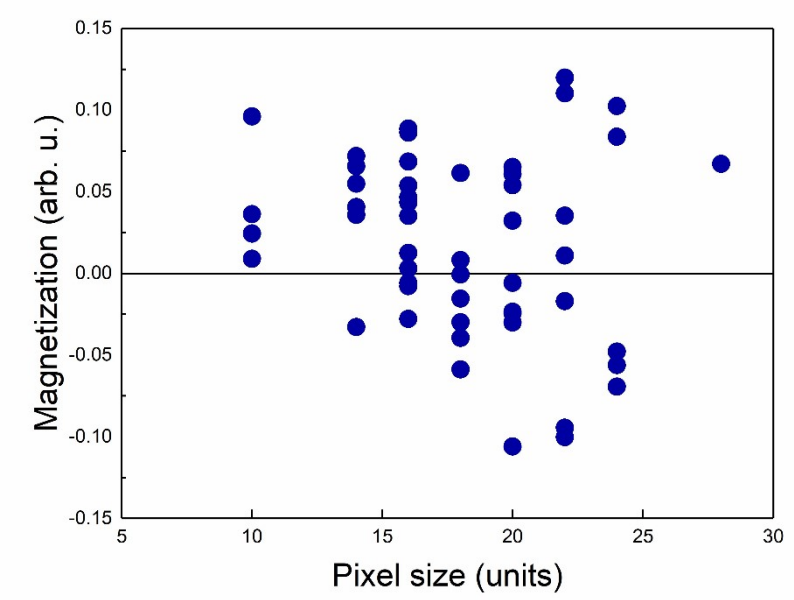

Figure S10. Normalized net magnetization m_z (within -1 and 1) of the selected 53 IONF in Figure 5(c) computed from the magnetic TXM images for polar angle $\theta = 0$ as a function of their diameter (in pixel units). They are nearly demagnetized, and no clear trend can be inferred, within the limited spatial resolution from TXM, from the cloud of points around zero magnetization as the diameter increases.

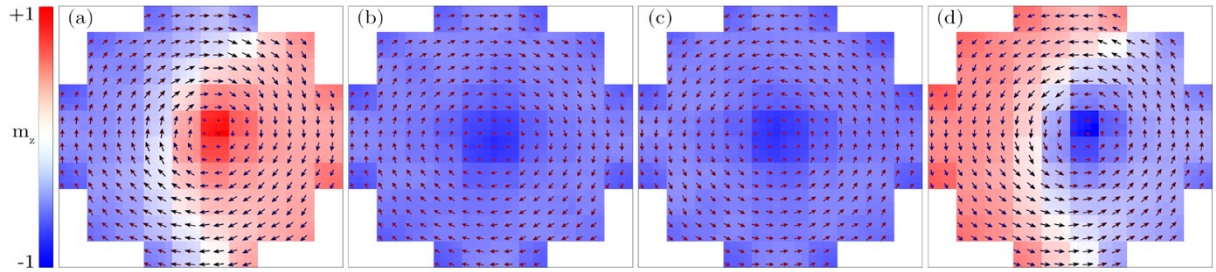

Figure S11. Moment maps in the equatorial plane of the IONF perpendicular to the z-axis for several applied fields and $A_i = 0.1A_w$. The cell color stands for the sign of the m_z component, and the arrow color has been arbitrarily chosen so that it shows high contrast with the cell color. (a) $H_z = 0$ kOe after saturation in the positive direction, (b) $H_z = -1.269$ kOe following the decreasing-field branch, (c) H_z −1.269 kOe after saturation in the negative direction, and (d) $H_z = 0$ kOe following the increasing-field branch.